

## Asymmetric mixing transport: A horizontal transport mechanism for sinking plankton and sediment in tidal flows

James M. Pringle<sup>1</sup> and Peter J. S. Franks

SIO-UCSD, Mail Stop 0218, La Jolla, California 92093-0218

### Abstract

A mechanism is described for the net horizontal transport of sinking plankton or sediment by oscillatory tidal flows. The mean motion of the plankton or particles is driven by the modulation of vertical mixing between flood and ebb. Cold water forced over warm water on the flood tide creates enhanced vertical mixing and resuspension of sinking particles higher into the water column. On ebb, the converse occurs, and sinking particles are lower in the water column. Since friction retards the tidal flow near the bottom, this leads to a net horizontal transport toward the less dense water. Because less dense water tends to be shallower, this will tend to move sinking plankton and sediment toward the crest of banks, toward the coast, and up embayments, even in the absence of any mean currents. A one-dimensional Eulerian model of this horizontal transport is developed and is compared to particle motion in a fully nonlinear two-dimensional model with an advanced turbulence closure scheme. The Eulerian model can, in most circumstances, predict the net horizontal motion of the particles as a function of their sinking speed and observable oceanographic properties. The mean horizontal speed of sinking particles is greatest when the sinking speed of the particles is about one-seventieth of the tidal velocities, or equivalently, about one-third of the mean turbulent velocity scale  $u^*$ . This horizontal transport of plankton and particles requires no behavior more complicated than simple sinking to achieve net horizontal speeds of several kilometers per day for realistic planktonic sinking speeds. It is possible that such a mechanism is a factor in larval recruitment and retention in coastal regions, for example, scallop larvae on Georges Bank.

Most benthic marine invertebrates have a planktonic larval stage that facilitates dispersal and gene flow between sessile or sedentary adult populations [Levin and Bridges 1995; McConaugh 1992]. To a large extent these larvae are at the mercy of the prevailing currents, often leading to a strong decoupling between adult fecundity and larval recruitment. Planktonic larvae are not completely passive, however, and even weak swimming behaviors can lead to significant horizontal transports when they interact with certain physical forcings. One striking example is the interaction of vertical migration with tidal flows leading to net transport (“selective tidal stream transport”; Wood and Hargis 1971).

Although most descriptions of physical–biological interactions leading to transport have invoked swimming behaviors of the plankton, there are some transport mechanisms that require nothing more complicated than plankton sinking. De Wolf (1973) described a mechanism allowing barnacle larvae to selectively move up an estuary: the larvae sank to the bottom on the ebb tide but were mixed into the water

column on the flood. The stronger currents on the flood tide were thought to cause this stronger vertical mixing, leading to enhanced resuspension of the sinking larvae. The net result was transport of these larvae up the estuary.

Georges Bank, a shallow and highly productive bank in the Gulf of Maine (Fig. 1), is characterized by mean cross-isobath currents that are only a small fraction of the strong tides sweeping the bank (Backus and Bourne 1987). If planktonic larvae spawned on the bank are to successfully recruit to the bank, they must remain on the bank despite the occasional storms that tend to remove waters from the bank (Gawarkiewicz 1993; Lewis et al. 1994). Many larvae, e.g., older scallop larvae, sink at speeds of order  $1 \text{ mm s}^{-1}$ , (Chia et al. 1984). To examine the impact of larval sinking on their retention on the bank, sinking and nonsinking particles were placed in the bottom boundary layer of a two-dimensional ( $x, z$ ) primitive equation model of Georges Bank developed and extensively compared to observations by Chen and Beardsley (1998). The particles that sank at  $1 \text{ mm s}^{-1}$  moved toward the crest of the bank much more rapidly than neutrally buoyant particles (Fig. 2). To the extent these particles are representative of scallop larvae, they indicate that sinking can help larvae remain on the bank and recruit to the adult populations on the flanks of the bank.

The observed transport of sinking particle in the two-dimensional model of Georges Bank motivated the study presented below. We begin by developing a simple, Eulerian, process-oriented model to diagnose the relevant dynamics. The source of the cross-isobath motions of sinking particles in a tidal flow is then discussed, and the speed of the motion is related to quantities observable in the field: the strength of the tides, the hydrography of the region, and the sinking speed of the particles. These theoretical predictions of the

<sup>1</sup> To whom correspondence should be addressed. Present address: Ocean Process Analysis Laboratory, Morse Hall 139, 39 College Road, Durham, New Hampshire 03824-3525 (jmpringle@ucsd.edu).

### Acknowledgments

We are pleased to acknowledge the help of Changsheng Chen and Claudio DiBacco, who aided in the modeling and biological intuition. Two reviewers greatly improved the text. This work was funded through grants to P.J.S.F. from NOAA for North Atlantic GLOBEC program, numbers NA76GP0176 and NA96OP0366. This is GLOBEC contribution number 172.

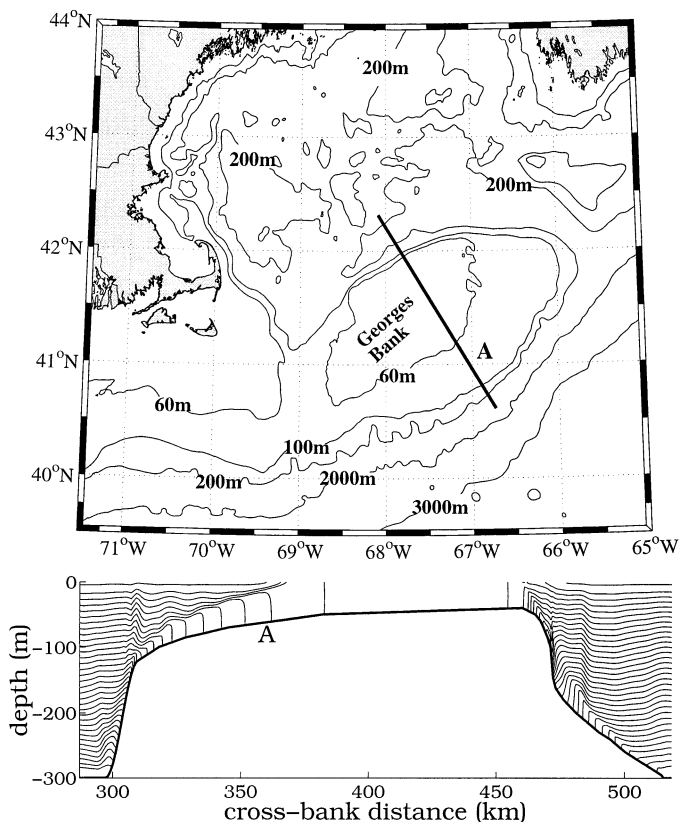


Fig. 1. Top: The bathymetry of Georges Bank and the surrounding regions. The thick dark line marks the approximate location of the two-dimensional model of Chen and Beardsley (1998, CB98 in the text). Bottom: The temperature at the beginning of the flood tide in the two-dimensional model. The contour interval is  $0.25\text{ }^{\circ}\text{C}$ . The model was run with their typical summertime stratification.

cross-isobath motions of the sinking particles are then compared to the motions of sinking particles in the two-dimensional primitive equation model of Georges Bank (Chen and Beardsley 1998; hereafter CB98) and the successes and failures of both the theory and the primitive equation numerical model identified. Particular attention is paid to where the Eulerian model is sufficient and to where a more complex Lagrangian model must be used to predict the horizontal motions of sinking particles. Finally, the biological ramifications of these cross-isobath motions are discussed.

### The asymmetric mixing transport mechanism

Tidal currents near the bottom are sheared vertically: horizontal velocities are stronger farther away from the bottom because of bottom friction. In a region of horizontal density gradient along the bottom, one phase of the tide (usually the flood) will drive dense water over less dense water (Fig. 3). This unstable density profile will convectively mix, causing enhanced turbulence and vertical mixing during this phase of the tide. On the opposite tidal phase (the ebb), the vertical density gradient is enhanced, suppressing vertical mixing. Sinking particles in such a flow will tend to be suspended higher in the water column during the flood than the ebb

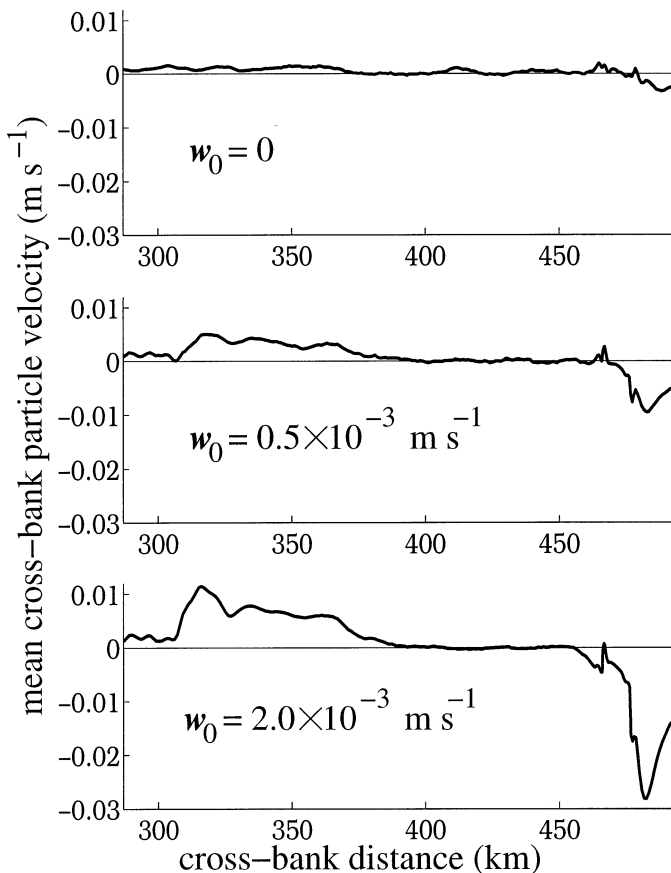


Fig. 2. The mean cross-isobath velocity of particles sinking with speed  $w_0 = 0, 0.5, \text{ and } 2 \times 10^{-3}\text{ m s}^{-1}$  for the summertime model of CB98. The cross-bank distances on the abscissa correspond to those in the bottom panel of Fig. 1. Positive values are to the right.

tide. This difference in distance from the bottom, combined with the vertical shear of the horizontal tidal currents, leads to a net transport in the direction of the less dense water. Thus, even if the currents have no mean over a tidal cycle, the particles have a mean motion toward the less dense water caused by the asymmetry in vertical mixing over a tidal cycle. We term this mechanism “asymmetric mixing transport.”

Figure 4 illustrates this mechanism for an arbitrary but representative point on the south flank of Georges Bank in the model of CB98 (marked A in Fig. 1). The cross-bank currents are nearly perfectly symmetric between flood and ebb, but the vertical mixing is stronger, and thus the average height of the particles greater, when the flow is onto the bank. This drives an on-bank motion at that point of  $3.5\text{ mm s}^{-1}$  for particles that sink at  $0.5\text{ mm s}^{-1}$  and an even greater  $5.5\text{ mm s}^{-1}$  ( $\approx 0.5\text{ km d}^{-1}$ ) for particles that sink at  $2\text{ mm s}^{-1}$ . If there is no sinking, the net cross-bank motion of plankton in the bottom boundary layer is only  $1.2\text{ mm s}^{-1}$ . Everywhere in the model the net motion of sinking particles is onto the bank because the least dense water is on the crest of the bank and can reach speeds of several centimeters per second on the flanks of the bank (Figs. 1 and 2). (The mean net motion and height of a particle was found by tracking

several hundred thousand particles in the bottom boundary layer of the model of CB98 over a tidal cycle. The Lagrangian particle tracking code in CB98 was modified to include sinking and the effects of turbulence on the particles, using the algorithm described by Visser 1997. The vertical diffusivity of temperature, computed from the Mellor-Yamada turbulence closure scheme CB98, was used as a proxy for turbulence.)

In order to understand how the mean cross-isobath particle velocity  $\langle u_{\text{eff}} \rangle$  depends on the strength of the tides, the sinking speed of the plankton or sediment, the mixing asymmetry, etc., it is convenient to develop a simple model of the mean particle motion. The model chosen is quasi-steady, i.e., it assumes that the vertical mixing, horizontal velocities, and particle concentrations adjust to the tidal forcing faster than the tidal period of about 12.42 h. These approximate solutions can be used to estimate the mean cross-isobath speed of particles,  $\langle u_{\text{eff}} \rangle$ .

These approximations are appropriate when the turbulent eddies in the bottom boundary layer mix water and momentum across the bottom boundary layer in much less than a tidal period. This is true when  $u^*$ , the velocity scale of the eddies in the bottom boundary layer, is large enough, and  $h_{\text{bb1}}$ , the thickness of the bottom boundary layer, is small enough, so that  $h_{\text{bb1}}/u^*$  is much less than a tidal period. The parameter  $u^*$  is related to the currents in the weakly stratified regions near the bottom by

$$\text{current speed} = \frac{u^*}{\kappa} \log\left(\frac{z + z_0}{z_0}\right), \quad (1)$$

where  $\kappa$  is von Karman's constant (0.4) and  $z_0$  is about one-tenth of the length scale of bottom roughness. (Derivations of Eq. 1 and discussions of  $z_0$  are found in basic fluid dynamics books, e.g., Kundu 1990 or Stull 1988, and discussions of the determination of  $z_0$  from data can be found in, e.g., Trowbridge and Lentz 1998.) Typical values of  $z_0$  are about  $10^{-3}$  m, giving a  $u^*$  of about one-twentieth the horizontal currents 10 m away from the bottom (Werner 1999). Georges Bank bottom boundary layers are 10s of meters thick (Fig. 1), and the tidal currents are about  $0.5 \text{ m s}^{-1}$ , implying an adjustment time scale of an hour or so, which is fast compared to the tides (Backus and Bourne 1987) (this also agrees well with observations of mixing time scales on the bank made by Horne et al. 1996.)

Neglecting rotation ( $u^*/[f \pm \omega_{\text{M2}}] < h_{\text{bb1}}$ ) and assuming that the boundary layer stratification is weak, the cross-shelf tidal velocity will then be approximately

$$u = \frac{u_{\text{ave}}^*}{\kappa} \log\left(\frac{z + z_0}{z_0}\right) [\gamma \cos(\omega_{\text{M2}}t) + \gamma_{\text{M4}} \cos(2\omega_{\text{M2}}t)], \quad (2)$$

where  $u_{\text{ave}}^*$  is the average turbulent velocity scale over a tidal period,  $\omega_{\text{M2}}$  is the M2 tidal frequency, and  $\gamma$  is the ratio of the peak cross-isobath velocity of a tidal constituent to the average current magnitude. For a purely M2 tide in a channel,  $\gamma = 1.6$ , or one over the average value of the absolute value of a cosine. For an ocean with an M2 rotary tide where the cross- and along-bank speeds are equal,  $\gamma = 1$ . For Georges Bank, where the along-bank tides are about half the cross-bank tides,  $\gamma \approx 1.2$ . The higher tidal frequency,  $\cos$

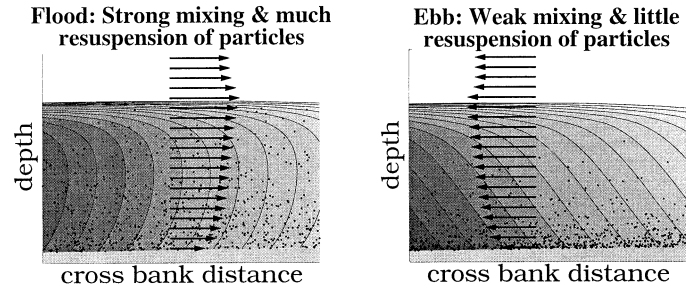


Fig. 3. A cartoon of an oscillating tidal flow in a bottom boundary layer with a horizontal temperature gradient (darker = colder, denser) and sinking particles. The shape of the isopycnals was taken from the model of CB98 at the point marked A on the lower panel of Fig. 1, but the strength of the tidal mixing asymmetry was tripled for emphasis.

( $2\omega_{\text{M2}}t$ ), results primarily from nonlinear advection and friction working on the M2 tides. It is negligible over most of Georges Bank (Backus and Bourne 1987) but can be important in estuaries (Jay and Musiak 1994). The relative phases of the two components will be seen below to be unimportant.

This simple model reproduces the vertical structure of the cross-bank flows in the bottom boundary layer over Georges Bank seen both in observations (Werner 1999) and in full numerical models (Fig. 5), particularly near the bottom where the assumptions that lead to a log-layer are most valid and the shear is strongest (Stull 1988). Since the mean particle motion is caused by turbulence resuspending particles in and out of this near-bottom region of high shear, its representation is particularly important.

Turbulence, which drives the resuspension of the sinking or downward-swimming particles, is modeled with a cubic mixing profile (Signell et al. 1990):

$$A = A_0 + \kappa u_{\text{ave}}^* \left( \frac{(z - h_{\text{bb1}})^2}{h_{\text{bb1}}} + \frac{(z - h_{\text{bb1}})^3}{h_{\text{bb1}}^2} \right) \times \left[ 1 + \delta A \frac{2z}{h_{\text{bb1}}} \cos(\omega_{\text{M2}}t) + \delta A_{\text{M4}} \frac{2z}{h_{\text{bb1}}} \cos(2\omega_{\text{M2}}t) \right], \quad (3)$$

where  $h_{\text{bb1}}$  is the thickness of the bottom boundary layer,  $A_0$  is a background mixing level whose physical significance is given below,  $\delta A_{\text{M4}}$  parameterizes the increased turbulence when the tides are running, and  $\delta A$  is the horizontal density gradient-induced mixing asymmetry in the middle of the bottom boundary layer. The cubic profile is chosen so the slope of the mixing profile near the bottom boundary is  $u^*\kappa$ , in agreement with Prandtl's law of the wall, and so the mixing goes smoothly to zero at the top of the bottom boundary layer. The mixing asymmetry increases linearly away from the bottom as a crude model of the increasing magnitude of the stratification away from the bottom, where, because diffusivity does not go exactly to zero, the stratification must be zero so there is no diffusive flux of density through the bottom. This vertical structure for the mixing asymmetry can be shown to be appropriate for the bottom two-thirds of the boundary layer in the limit of small Richardson number.  $\delta A$  can be estimated from observations of the temporal varia-

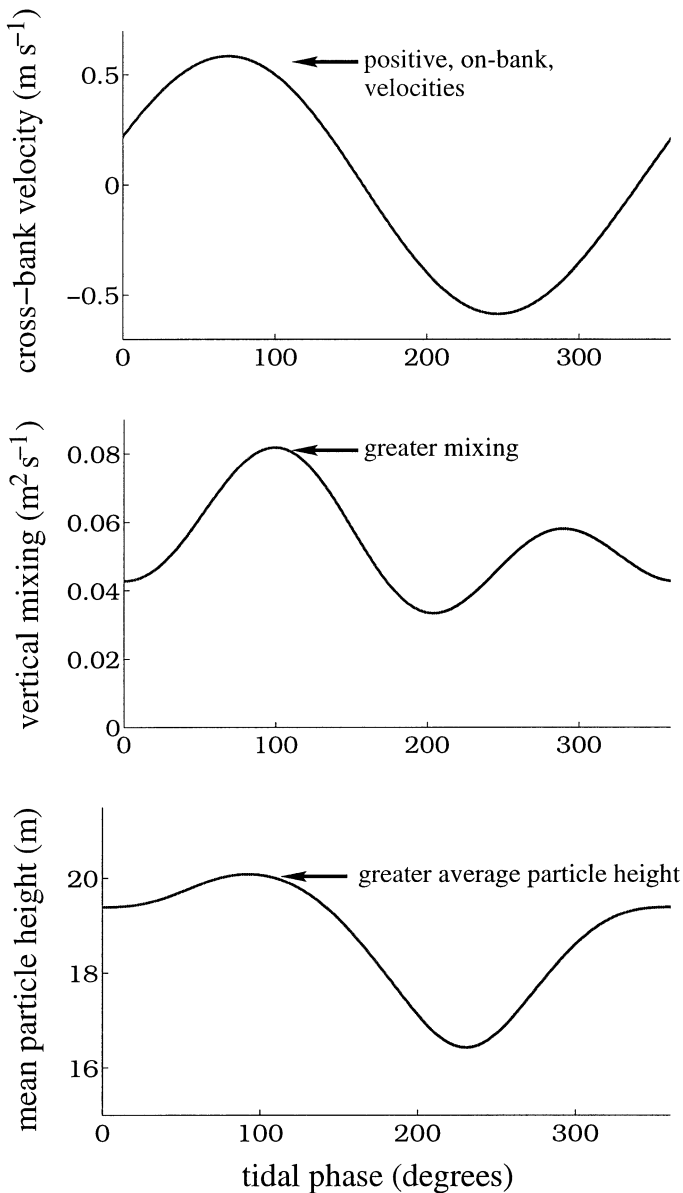


Fig. 4. The cross-isobath currents and vertical mixing coefficient in the middle of the bottom boundary layer (23.5 m above bottom) and the mean height of particles above the bottom for the model of CB98 at the point marked A on the lower panel of Fig. 1. The particles sank at a speed of  $1 \text{ mm s}^{-1}$ .

tions in the gradient Richardson number in the middle of the bottom boundary layer, using a rather ad hoc turbulence closure in which  $\delta A$  is about five times the maximum Richardson number in the middle of the bottom boundary layer (Geyer 1995; Villaret and Trowbridge 1991). Since the Richardson number is difficult to measure in the field, it will often be easier to use the observed tidal currents and horizontal and vertical density gradients as forcing for a one-dimensional vertical model with a realistic turbulence closure, as done by Nunes Vas and Simpson (1994), and then to recover  $\delta A$  from the model. Figure 6 compares Eq. 3 with the model of CB98 at station A of Fig. 1. The cubic mixing profile captures the slope of mixing strength near the bottom,

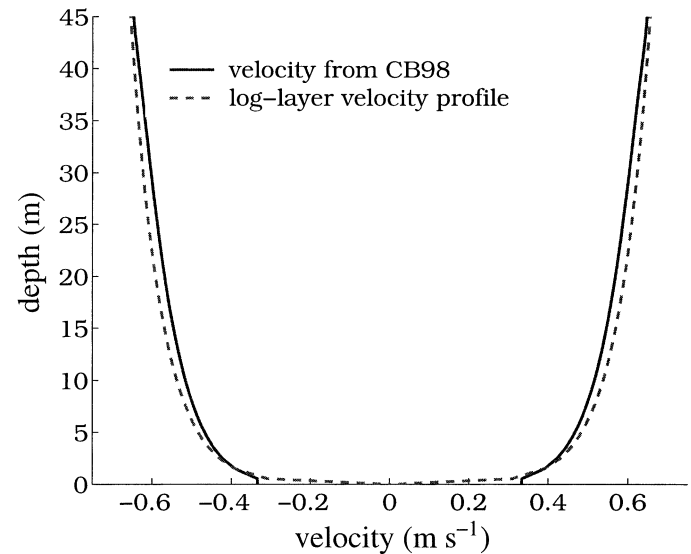


Fig. 5. The cross-isobath velocity in the bottom boundary layer at point A of Fig. 1 when the velocity near the bottom is at peak flood and ebb for both the model of CB98 and Eq. 2. The turbulent velocity scale  $u^* = 0.02 \text{ m s}^{-1}$ .

where the current shears are greatest and realism most important, but somewhat overestimates the mixing in the interior.

The parameter  $\delta A_{M4}$  reflects the increased vertical mixing when the tidal currents are greatest at full flood and ebb. Since the vertical turbulent mixing scales linearly with current speed (if  $\delta A$  is small),  $\delta A_{M4}$  should scale as the M4 amplitude of the tidal speed (not velocity). This will range from 0, when the tidal ellipse is a circle and thus the speed never varies, to 0.5 for a rectilinear tidal current. On Georges Bank,  $\delta A_{M4} \approx 0.25$ . It has been assumed above that this modulation decreases near the bottom in order to reduce the

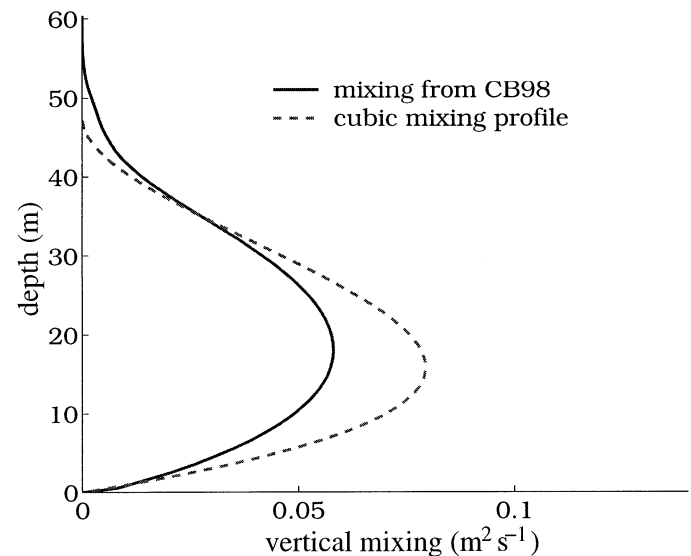


Fig. 6. The tidal cycle mean vertical mixing at point A of Fig. 1 from the model of CB98 and Eq. 3. The thickness  $h_{\text{bb1}} = 47 \text{ m}$ ,  $A_0 = 10^{-3} \text{ m}^2 \text{ s}^{-1}$ , and  $u^* = 0.02 \text{ m s}^{-1}$ .

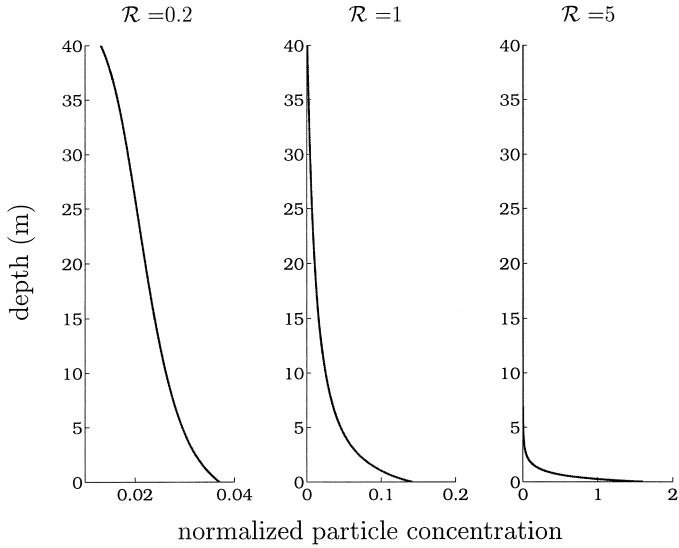


Fig. 7. The vertical profile of normalized particle concentration for  $\mathcal{R} < 1$ ,  $\mathcal{R} = 1$ , and  $\mathcal{R} > 1$  from Eq. 5 for  $\delta = 1$ . The sinking speed  $w_0$  equals 1.6, 8.2, and 41 mms  $s^{-1}$ , respectively. The thickness  $h_{bb1} = 40$  m,  $A_0 = 2 \times 10^{-2}$   $s^{-1}$ , and  $u^* = 0.02$  m  $s^{-1}$ .

algebraic complexity of the following solution. Although this assumption is not accurate, it allows the relative importance of overtimes to be judged. Relaxing this assumption does not quantitatively change the result.

Given the diffusivity, Eq. 3, and a steady-state advection–diffusion equation for the vertical distribution of particles sinking or swimming downward at a speed  $w_0$ ,

$$w_0 \frac{\partial c}{\partial z} = \frac{\partial}{\partial z} A \frac{\partial c}{\partial z} \quad (4a)$$

$$w_0 c = A \frac{\partial A}{\partial z} \quad \text{at } z = 0, h_{bb1}, \quad (4b)$$

the particle concentration  $c(z)$  is

$$c(z) = c_0 \times \exp \left[ h_{bb1}^3 w_0 \sum_{\lambda} \left( -8z A_0 h_{bb1}^5 \Delta \kappa u_{ave}^* \lambda^2 - 2z \right. \right. \\ \left. \left. + 4u_{ave}^* \kappa \Delta A_0 h_{bb1}^6 \lambda^2 \right. \right. \\ \left. \left. - 8A_0 h_{bb1}^3 \lambda + h_{bb1} \right) \right], \quad (5a)$$

where

$$\Delta = 1 + \delta A \cos(\omega_{M2} t) + \delta A_{M4} \cos(2\omega_{M2} t), \quad (5b)$$

$\lambda$  are the roots of

$$0 = (16A_0^2 h_{bb1}^1 \Delta^2 \kappa^2 u_{ave}^{*2} + 256A_0^3 h_{bb1}^9 \Delta \kappa u_{ave}^*) \lambda^4 \\ + 8u_{ave}^* \kappa \Delta A_0 h_{bb1}^5 \lambda^2 + 1, \quad (5c)$$

and  $c_0$  is chosen so the integral of Eq. 5 over the water column is one and dimensionless. This formula, the Rouse profile, and many variations on it, are discussed in much greater detail in, e.g., Fredsoe and Deigaard (1992). The Rouse profile is controlled by one nondimensional number, the Rouse number  $\mathcal{R} = -w_0 / (\kappa u_{ave}^*)$ , whose role can be un-

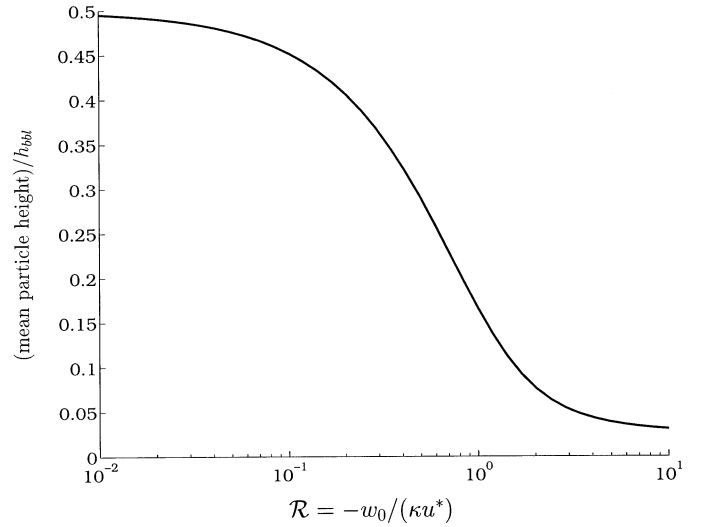


Fig. 8. The mean height of a particle normalized by the boundary layer thickness  $h_{bb1}$  as a function of the Rouse number  $\mathcal{R}$ ,  $z_r/h_{bb1}$  is 0.025.

derstood in its limits (shown in Fig. 7 for  $\Delta = 1$ ). When the sinking speed  $w_0$  is large or the turbulent velocity  $u^*$  is small,  $\mathcal{R}$  is greater than one and the particles are concentrated near the bottom. As turbulence increases or  $w_0$  decreases,  $\mathcal{R}$  becomes less than one and the particles are spread throughout the water column. The average height of a particle approaches half the boundary layer thickness as  $\mathcal{R}$  becomes less than one, and  $A_0/w_0$  as  $\mathcal{R}$  becomes greater than one (Fig. 8). As the tidal currents go to zero, the particles will remain suspended a distance  $z_r = A_0/w_0$  off the bottom. This is an artifice intended to parameterize the effects of the initial resuspension of particles—as  $u^* \kappa$  becomes somewhat less than  $w_0$ , real particles will tend to settle out onto the bottom and only be transported by bed-load processes (Fredsoe and Deigaard 1992, section 7.4, Emerson 1991). In the ocean, as  $\kappa u^*$  exceeds a value of  $\approx w_0$  the particles are initially resuspended some height  $z_r$  above the bottom—perhaps two particle widths over a smooth bottom, or several ripple heights over a sandy bottom with sand ripples (Fredsoe and Deigaard 1992). In that case,  $z_r$  is specified and  $A_0$  is set to  $w_0 z_r$ . If there is a strong surface-wave field, the particles can be continuously resuspended near the bottom, even in the absence of a mean flow, and  $A_0 = 0.0752 A_w \omega h_r$ , where  $A_w$  is the wave orbital excursion near the bottom,  $\omega$  is the frequency of the surface wave field, and  $h_r$  is approximately the bottom ripple height (Williams et al. 1999). The resuspension height  $z_r$  is not allowed to vary with the phase of the tide because the resuspension is driven by very near-bottom mechanically forced turbulence, which will not feel the effects of stratification that only exists higher in the water column (e.g., Stull 1988).

Given the horizontal water velocity and the vertical profile of particle concentration, the depth- and tidal-mean cross-bank velocity of the particles  $\langle u_{eff} \rangle$  can be calculated:

$$\langle u_{eff} \rangle = \frac{\omega_{M2}}{2\pi} \int_0^{2\pi\omega_{M2}^{-1}} dt \left( \int_0^{h_{bb1}} uc \, dz \right). \quad (6)$$

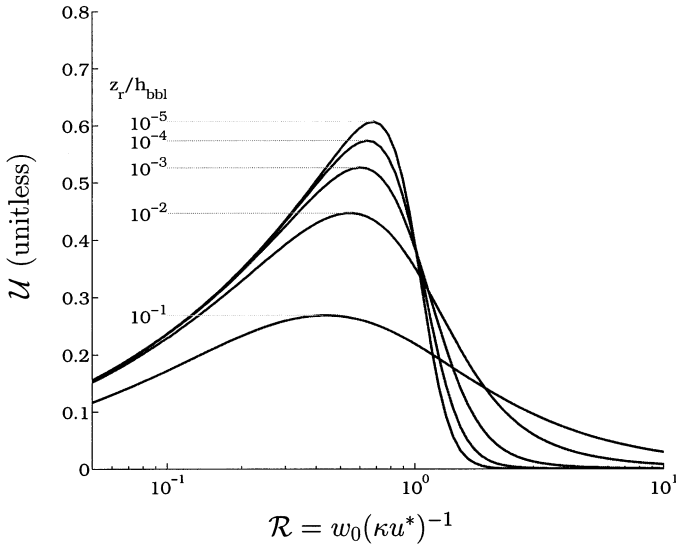


Fig. 9.  $\mathcal{U}$  as a function of  $\mathcal{R}$  for various values of  $z_r/h_{bb1}$ .

The quasi-steady models for the cross-bank velocity Eq. 2 and the vertical distributions of particles Eq. 5 can then be substituted into Eq. 6 to obtain an estimate of  $\langle u_{\text{eff}} \rangle$ :

$$\langle u_{\text{eff}} \rangle = \frac{\omega_{M2}}{2\pi} \int_0^{2\pi\omega_{M2}^{-1}} dt \left( \frac{\gamma u_{\text{ave}}^*}{\kappa} \Gamma \right) \quad (7a)$$

$$\Gamma = \int_0^{h_{bb1}} dz \left\{ \log \left( \frac{z + z_0}{z_0} \right) c(z, \Delta) \right\} \quad (7b)$$

( $\Delta$  is as in Eq. 5). This expression for  $\langle u_{\text{eff}} \rangle$  is analytically intractable because the integral for  $\Gamma$  is difficult to solve in closed form. However, if  $\delta A$  is small compared to one,  $\Gamma$  can be written as the first two terms of a Taylor series

$$\Gamma = \Gamma_0 + \delta A \cos(\omega_{M2}t)U + \delta A_{M4} \cos(2\omega_{M2}t)U, \quad (8)$$

where  $\Gamma_0$  is Eq. 7b evaluated with  $\Delta = 1$  and  $\mathcal{U}$  is

$$U = \left. \frac{\partial \Gamma}{\partial \Delta} \right|_{\Delta=1}. \quad (9)$$

Eq. 7 then becomes, for small  $\delta A$ ,

$$\langle u_{\text{eff}} \rangle = \frac{1}{2} \frac{u_{\text{ave}}^*}{\kappa} U (\gamma \delta A + \gamma_{M4} \delta A_{M4}) \quad (10)$$

(The error in this approximation remains less than 50% if  $\delta A$  remains less than 0.6).

$\mathcal{U}$  is still not solvable in closed form, but it depends only on a small number of parameters:  $u^*$ , the turbulence velocity scale;  $w_0$ , the particle sinking speed;  $h_{bb1}$ , the bottom boundary layer thickness;  $z_0$ , the bottom roughness; and  $z_r$ , the resuspension height of the particles (defined as  $A_0 w_0^{-1}$  above). Furthermore, as can be verified by the direct numerical evaluation of Eq. 7b,  $\mathcal{U}$  does not depend on  $z_0$  when  $z_0/z_r < 1$ . This leaves four parameters in two units, length and time, so  $\mathcal{U}$  must depend on only two dimensionless parameters (Kundu 1990, chapter 8). Given the discussion above, the Rouse number  $\mathcal{R} = -w_0/(\kappa u^*)$  is chosen for one of the parameters. The other parameter is then  $z_r/h_{bb1}$ , the

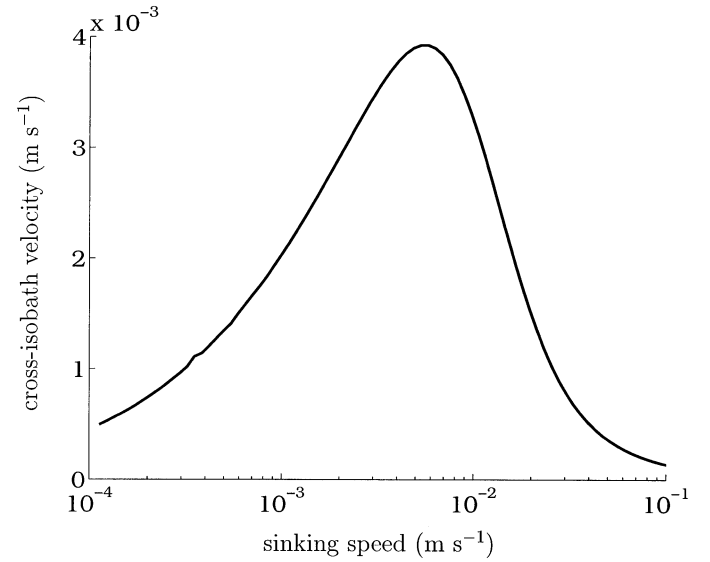


Fig. 10. Mean cross-isobath velocity  $\langle u_{\text{eff}} \rangle$  as estimated from Eq. 7 for station A of Fig. 1.

ratio of the initial particle resuspension height to the thickness of the bottom boundary layer.  $\mathcal{U}$  is shown in Fig. 9 as a function of these two parameters.

From Eq. 10, it can be seen that the overtides can be neglected if  $\gamma \delta A$  is much greater than  $\gamma_{M4} \delta A_{M4}$ , as is true on Georges Bank. Overtides will thus not be discussed below.

#### How Eq. 10 is used: Application to Georges Bank

Eq. 10 allows the mean cross-isobath motion to be determined as a function of quantities that can be observed in the field: the strength of the tides  $u_{\text{ave}}^*$  and  $\gamma$ , the mixing asymmetry  $\delta A$  and  $\delta A_{M4}$ , the thickness of the bottom boundary layer  $h_{bb1}$ , and the particle resuspension height  $z_r$ . An example is given below for a numerical model of Georges Bank, all of whose flow fields have been tuned to reproduce those on the actual bank. (The use of the numerical model as an intermediate step may seem odd here, but it will be useful later in quantifying the errors in the simple model presented above.)

The net horizontal velocity of sinking particles,  $\langle u_{\text{eff}} \rangle$ , can be estimated for station A of Fig. 1 for any sinking speed  $w_0$  by taking  $\delta A = 0.24$ ,  $u_{\text{ave}}^* = 0.02 \text{ m s}^{-1}$ ,  $\gamma = 1.2$ , and  $z_r/h_{bb1} = 0.02$  from the model of CB98, and estimating  $\mathcal{U}$  from Fig. 9. (In a numerical model like that used in CB98,  $z_r$  is the vertical extent of the bottommost grid cell, since all particles near the bottom experience horizontal currents appropriate to that height. Here,  $z_r \approx 1 \text{ m}$ .) The curve of  $\mathcal{U}$  is then multiplied by  $\delta A$ ,  $u_{\text{ave}}^*$ , and  $\gamma$  and divided by 2 and  $\kappa = 0.4$  to produce the estimate of  $\langle u_{\text{eff}} \rangle$  in Fig. 10. For this location on Georges Bank, maximal values of  $\langle u_{\text{eff}} \rangle$  are about  $0.4 \text{ cm s}^{-1}$ , or about a third of a kilometer a day. The parameter  $\langle u_{\text{eff}} \rangle$  is largest when the downward speed of the plankton or particle is about  $0.7 \kappa u^*$  and  $\mathcal{R} \approx 0.7$ , in this case about  $0.7 \text{ cm s}^{-1}$ . This maximum of  $\langle u_{\text{eff}} \rangle$  occurs because when  $\mathcal{R} \approx 1$  small changes in the turbulence lead to large changes in the average height of a particle off the bottom

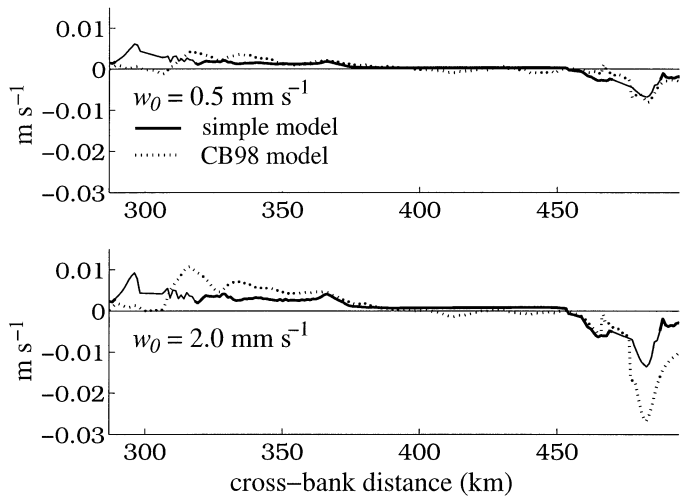


Fig. 11. Cross-isobath motion due to sinking for particles sinking at  $w_0 = 0.5$  and  $2 \times 10^{-3}$   $\text{m s}^{-1}$  as estimated by Eq. 10 and seen in the model of CB98 for Georges Bank. To concentrate on the cross-bank motion induced by sinking, the speed of nonsinking particles in the bottom boundary layer has been removed from the sinking particles in the model of CB98 (i.e., the top panel of Fig. 2 has been subtracted from the bottom two panels in order to produce the dashed lines above). The line for the estimate of  $\langle u_{\text{eff}} \rangle$  is thin where  $\delta A > 0.6$  and the Taylor series expansion of Eq. 7b is unreliable.

(Fig. 8). It is this change in the average height of the particles between flood and ebb that lifts the particles in and out of the slower flows near the bottom, causing  $\langle u_{\text{eff}} \rangle$ . As seen in Fig. 7, when  $\mathcal{R} \gg 1$  the particles are all resting on the bottom, regardless of any minor changes in the mixing, and when  $\mathcal{R} \ll 1$  the particles are evenly spread through the bottom boundary layer, again unaffected by any minor changes in the strength of the turbulent mixing. Thus in both these limits  $\langle u_{\text{eff}} \rangle$  is small.

Equation 10 can also be applied to the entire bank and used to explain the structure of  $\langle u_{\text{eff}} \rangle$  on Georges Bank. In the model of CB98, for particles sinking at  $0.5$  and  $2 \times 10^{-3}$   $\text{m s}^{-1}$ ,  $\langle u_{\text{eff}} \rangle$  is always toward the shallowest portion of the bank and is larger where the bathymetry is steepest but becomes nearly zero at the shallowest, flattest, portion of the bank (Fig. 11). According to Equation 10,  $\langle u_{\text{eff}} \rangle$  is linearly proportional to  $u^*$ ,  $\delta A$ , and  $\mathcal{R}$ .  $\mathcal{R}$  in the model varies little across the bank, from about  $0.4$  to  $0.2$ , except on the steepest portions of the bank, so changes in  $\mathcal{R}$  do not dominate the variation of  $\langle u_{\text{eff}} \rangle$  across the bank (Fig. 12). The parameter  $u^*$ , which is proportional to  $\mathcal{R}^{-1}$ , is at its greatest in the shallowest portion of the bank where  $\langle u_{\text{eff}} \rangle$  is least, so it too cannot explain the variation in  $\langle u_{\text{eff}} \rangle$ . The parameter  $\delta A$ , however, is greatest on the flanks and smallest over the crest of the bank (Fig. 12) and explains the variation in  $\langle u_{\text{eff}} \rangle$  well. Having isolated  $\delta A$  as the most important parameter controlling  $\langle u_{\text{eff}} \rangle$ , it is now only necessary to explain the variation in  $\delta A$  to explain the variation in  $\langle u_{\text{eff}} \rangle$ . In the simple heuristic presented above, cross-isobath density gradients are invoked to explain the tidal mixing asymmetry and  $\delta A$  increases as bottom boundary layer horizontal density gradients increase. This agrees with the results of CB98: the var-

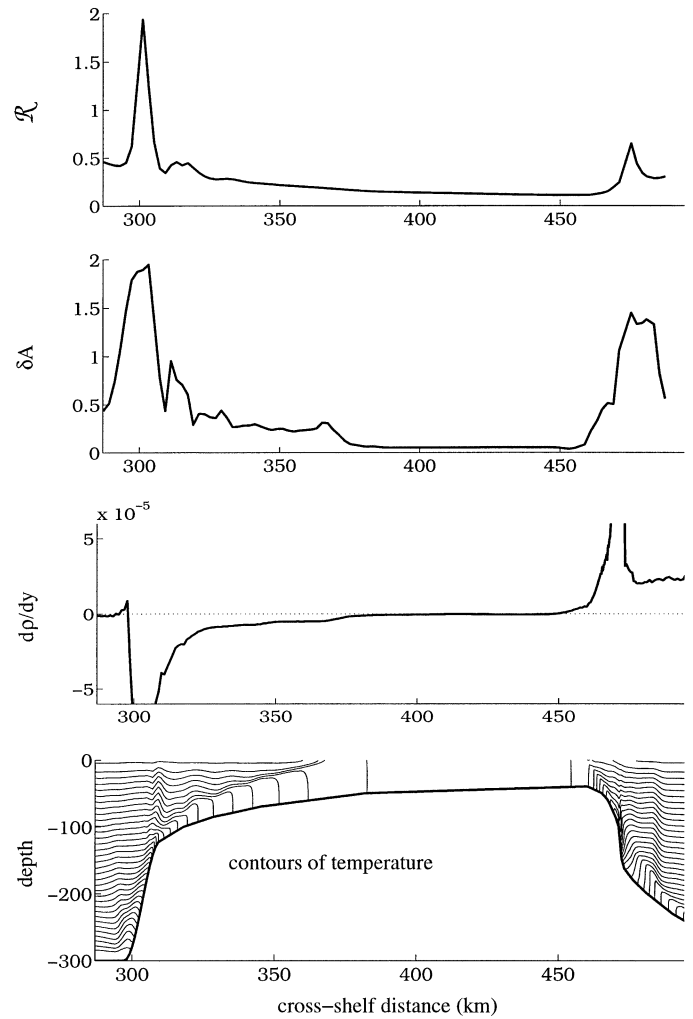


Fig. 12. From top to bottom:  $\mathcal{R}$  for  $w_0 = 2 \times 10^{-3}$   $\text{m s}^{-1}$ ,  $\delta A$ , the horizontal density gradient in the bottom boundary layer, and the temperature in the model of CB98 (the contour interval is  $0.2^\circ\text{C}$ ).  $\delta A$  is calculated as the vertical average over the bottom boundary layer of the ratio of the M2 component of vertical mixing to the time mean vertical mixing and thus can be greater than one where the vertical mixing is only strong for a brief portion of the tidal cycle.

iation of  $\delta A$  across the bank mirrors the magnitude of the horizontal density gradients. The cross-isobath density gradient arises from the interaction of tidal mixing, bottom topography, and stratification. Stronger stratification or, as in CB98, stronger bottom slopes increase cross-isobath density gradients. This increases  $\delta A$  and the cross-isobath motion of sinking particles where the bottom is steeply sloped and explains why there is little particle transport across the nearly flat crest of the bank.

#### Where else might asymmetric mixing be important

In regions of sloping bottom topography, strong tidal currents, and strong stratification, the mechanisms described in the previous sections will conspire to generate a density gradient in the bottom boundary layer so that the less dense

water is toward the shallows. When the mean cross-isobath flows are weak and the cross-isobath tides are strong, asymmetric mixing transport is likely to be an important mechanism for upslope transport of sinking particles. Such regions include nonestuarine embayments, mixing dominated estuaries, banks, and shoals. (In many estuaries, overtides will also be important and the  $\gamma_{M4}\delta A_{M4}$  term in Eq. 10 will dominate. The transport driven by the overtides, known as “settling-lag transport,” is described in, e.g., Jay and Musiak 1994, and can be estimated with Eq. 10.)

In non-tidal-mixing dominated estuaries, the fresh water discharge will tend to drive strong landward mean flows near the bottom, which will usually be more important than the asymmetric mixing mechanism (Hansen and Rattray 1965).

#### Sources of error in the estimates of $\langle u_{\text{eff}} \rangle$

A comparison of the quasi-steady approximation for  $\langle u_{\text{eff}} \rangle$ , Eq. 10, to the on-bank motion of sinking particles in the primitive equation numerical model of Georges Bank (CB98; Fig. 11) shows that our simple model gives a reasonable approximation of particle transports. The error in  $\langle u_{\text{eff}} \rangle$  is generally less than a factor of two, except for the steepest portions of the bank, on the northern and southern flanks, where the error can be much greater.

There are two sources of error in the quasi-steady estimation of  $\langle u_{\text{eff}} \rangle$ : (1) the simple models for vertical mixing (Eq. 3) and cross-isobath velocities (Eq. 2) may not be adequate, or (2) the motion of sinking particles may not be determined solely by the currents and mixing at a single location but by the variation of the currents and mixing experienced by a particle as it moves across the bank over a tidal cycle.

In order to separate these two possible sources of error,  $\langle u_{\text{eff}} \rangle$  is recalculated from Eqs. 4 and 6, but with demeaned cross-isobath currents and vertical-mixing coefficients taken from a single location in the numerical model, resulting in a new estimate,  $\langle u_{\text{eff}} \rangle_{\text{CB98}}$  (the mean of the model currents is removed because it is nearly balanced by a Stokes drift, Chen and Beardsley 1998). The parameter  $\langle u_{\text{eff}} \rangle_{\text{CB98}}$ , like the estimate of  $\langle u_{\text{eff}} \rangle$  in Eq. 10, is an Eulerian estimate because it uses the currents and mixing at one horizontal location instead of the currents and mixing experienced by the particles as they move over a full tidal excursion. Where  $\langle u_{\text{eff}} \rangle_{\text{CB98}}$  agrees with the  $\langle u_{\text{eff}} \rangle$  found by tracking particles in CB98 but disagrees with the estimate of  $\langle u_{\text{eff}} \rangle$  from Eq. 10, the error must lie in the approximations for the currents and vertical mixing given in Eqs. 2 and 3. Where both  $\langle u_{\text{eff}} \rangle_{\text{CB98}}$  and Eq. 10 fail to predict the motions of particles in the model of CB98, the errors must come from failing to include Lagrangian effects, i.e., using the currents and mixing from one location, instead of using the mixing and currents experienced by the particles as they sweep back and forth across the bank over a tidal cycle. Because for most of the bank,  $\langle u_{\text{eff}} \rangle_{\text{CB98}}$  agrees well with  $\langle u_{\text{eff}} \rangle$  from Eq. 10 (Fig. 13), most of the error in the estimation of  $\langle u_{\text{eff}} \rangle$  must come from neglecting Lagrangian effects (the one exception to this occurs where  $x < 295$  km, where the bottom becomes flat again).

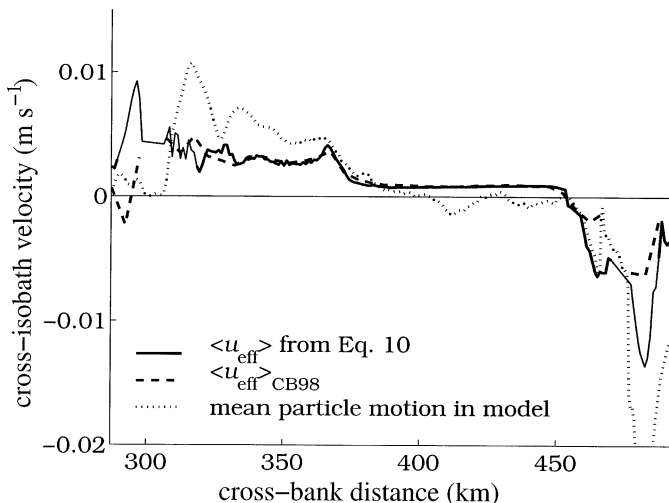


Fig. 13. The mean motion of particles in the model of CB98,  $\langle u_{\text{eff}} \rangle$  from Eq. 10 and  $\langle u_{\text{eff}} \rangle_{\text{CB98}}$  for particles sinking at  $0.5 \times 10^{-3} \text{ m s}^{-1}$ .

The error is greatest on the steep flanks of the bank, indicating that the spatial variations in currents and mixing across the bank are important there. Close examination of the model output shows that the phase of the currents changes rapidly over the steepest portion of the bank because of the interaction of the bathymetry with the stratification and the consequent generation of internal waves (for details, see CB98). Lagrangian motions are most likely to be important where the path of a particle over a tidal cycle encompasses  $O(1)$  changes in depth. However, even in the regions where the Eulerian model is poor, asymmetric mixing and sinking enhances the cross-bank transport of particles.

#### Errors in the primitive equation model's estimate of $\langle u_{\text{eff}} \rangle$

In the section above, and in Figs. 2, 11, and 13, the sinking speeds of the particles were such that  $\mathcal{R} < 1$  everywhere (except for a very small portion of the south flank). This was done because the model of CB98 and most other modern numerical models are incapable of correctly simulating the motions of particles whose sinking/downward swimming speed is fast enough that they are concentrated near the bottom, which occurs when  $\mathcal{R} \approx > 1$  (Fig. 8).

Since numerical models are often used to understand larval motions, it is useful to understand why they can fail to reproduce the motion of sinking particles and how these failings can be fixed. The models have two failings, one minor and one major. The minor failing is the model's inability to properly reproduce the resuspension of particles, especially by surface wave-generated turbulence. This failure is minor because it can be remedied by adding a small extra diffusivity to the model whose role is exactly analogous to  $A_0$  in Eq. 3. The extra diffusivity could be enabled only when the bottom stress exceeded a critical resuspension threshold, in cases where that was appropriate (Fredsoe and Deigaard 1992).

The more important failing of standard numerical models

is their inability to resolve the bottom log-layer in the one or two gridcells above the bottom. In order to do so they would have to have impractically fine vertical resolution. This failure does not affect the velocity dynamics, for the log-layer is a constant stress layer that can be parameterized with a drag law, as is done in all modern ocean circulation models. In these models, the horizontal velocity in the grid-cell nearest the bottom is the average velocity for that grid-cell: any particle within the bottom gridcell experiences the same velocity, regardless of its height above the bottom (see the bottom of Fig. 5). This is equivalent to saying that the particle resuspension height  $z_r$  is always the vertical resolution of the model. When  $\mathcal{R} > 1$ , the particles are concentrated in the bottommost part of the bottom gridcell and advecting them with the average velocity of the bottom gridcell is problematic. This is exacerbated in the model of CB98 because the vertical resolution varies inversely with the water depth—it is always one-sixtieth of the water depth. Thus particles with  $\mathcal{R} > 1$  experience a  $z_r$  that is inversely proportional to the water depth, leading to strong but spurious on-bank motions that are independent of the sinking speed.

In order to use rapidly sinking particles in an ocean circulation model, some functional form for the mixing and horizontal velocities in the bottom gridcell would have to be assumed (presumably similar to Eqs. 2 and 3), and these used to interpolate the horizontal velocity and mixing at the bottom gridpoint to the location of the particle.

### Biological implications

Asymmetric mixing transport provides a mechanism for plankton to maintain directed motion of up to a few kilometers per day with no expenditure of energy. It is not clear how such a transport could be verified in the field, but it is possible that some organisms display the necessary behaviors to exploit it. Most planktonic organisms larger than about 0.1 mm are more dense than water and will tend to sink. In particular, the eggs of many invertebrates and vertebrates sink with speeds of 10s to 100s of meters per day. The eggs of many species of copepod, for example, will reach the bottom before hatching (e.g., Tang et al. 1998, and references therein), sinking at 0.1–1 mm s<sup>-1</sup>. When entrained into the bottom boundary layer, these eggs could experience significant up-slope transport. Such a mechanism could be particularly important for meroplanktonic species in which the planktonic larvae need to recruit to benthic nearshore habitats. Most benthic marine invertebrates are meroplanktonic, with the potential for their larvae to be transported up-slope by this asymmetric mixing transport mechanism.

Adult scallop populations on Georges Bank are concentrated along the flanks of the bank, particularly the northeast peak. The scallop beds tend to lie under the region where the pycnocline intersects the bottom. As the tide moves the tidal fronts back and forth, the scallop beds can be under either stratified or well-mixed waters. According to the theory presented above, it is in this region that the up-flank, on-bank transport of sinking plankton would suddenly decrease due to the loss of the horizontal density gradient that causes the mixing asymmetry. The asymmetric mixing trans-

port could be a mechanism to retain scallop larvae on the flanks of the bank and enhance recruitment to the adult scallop beds, which appear to be somewhat self-seeding (Trembley 1991). But do the scallop larvae have the appropriate behavior?

Manuel et al. (1996) examined the vertical migration patterns of scallop larvae from three disparate populations, including one from Georges Bank. All larvae showed a diel vertical migration pattern, with more larvae near the surface during the night. They found that the Georges Bank larvae had distinctly different behaviors (apparently genetically determined) than the other populations, tending to be lower in the water column and making deeper excursions during the day after the age of 20 d or so. Veligers ready to settle were found throughout the water column, rather than concentrated in the surface waters. However, with a weaker thermocline, all larvae tended to be distributed throughout the water column and to settle in greater numbers with increasing depth. In a mesocosm study examining the effects of thermoclines and turbulence on scallop larvae, Pearce et al. (1998) showed increasing spat recruitment with depth in low turbulence intensities but more random with depth at higher levels of turbulence. Their observations were consistent with other studies in which larvae tended to move toward the bottom as they approached competency (Culliney 1974; Gallagher et al. 1996). This behavior would tend to move older larvae on-bank toward the tidal front through asymmetric mixing transport. Given the strong vertical migration behavior of the younger larvae, however, it is unlikely that the younger larvae would exploit asymmetric tidal mixing to move on-bank.

The distribution of inert sedimentary particles might be expected to follow the distribution of plankton exploiting the asymmetric mixing transport. De Wolf (1973) based his hypotheses of larval barnacle behavior on the correlation between barnacle concentrations and suspended sediments. Figure 10 suggests that on Georges Bank, a sinking velocity of about 1 cm s<sup>-1</sup> would lead to the strongest on-bank transports. Such sinking speeds are more characteristic of sands than silts and clays. The crest of Georges Bank (the region within the 60 m isobath) is covered by medium-to-coarse sands and gravel, whereas the flanks of the bank show slightly finer sands (Twichell et al. 1987). Moving farther off-bank, the sediments become finer silts and clays. Such a distribution is consistent with a winnowing and off-bank transport of the fine sediments by the strong tidal- and storm-driven currents on the bank, and possible transport of the sands onto the bank. There are regions along the northern flank and northeastern peak of Georges Bank where there is an abrupt transition from sands to coarser gravels beneath the tidal fronts, consistent with the asymmetric mixing transport mechanism. An important caveat is necessary, however, when using sediment to understand larvae recruitment—sediment exists for a long time, and so its distribution may be governed by rare but powerful events, such as winter storms (Twichell et al. 1987). Larvae, which must recruit or die in a few short weeks, will be more influenced by continual processes, such as asymmetric mixing.

Although we do not have any evidence that the asymmetric mixing mechanism is responsible for the location, du-

ration, or strength of larval recruitment or benthic plankton transport, we feel that it is a mechanism worth exploring in field studies. Quantification of such a transport will be difficult, but may be possible with the development and deployment of new molecular technologies for identifying and quantifying organisms. We have proposed measurable quantities to assess the probable strength of asymmetric mixing transport and discussed the likely sources of error in our simple model. It remains to address the relative importance of such a mechanism in a variety of field settings.

## Conclusion

If sinking or downward-swimming plankton reside in a bottom boundary layer in which there are no mean flows but strong oscillatory tides, they may nevertheless be transported across isobaths because of asymmetric vertical mixing induced by horizontal density gradients in the bottom boundary layer. The vertical mixing will be stronger when the tides are running from regions of dense water toward the less dense waters. This lifts sinking particles away from the bottom into swifter waters and thus causes a mean motion of the particles toward the less dense water. The horizontal density gradients that generate the tidal asymmetry in vertical mixing can arise for a variety of reasons; those generated by the mixing of vertical stratification will tend to generate a density gradient pointing toward the shallow waters, and thus sinking particles will tend to move toward the shallow waters.

When the distance a particle travels in half a tidal period does not encompass order one variations in depth, Eulerian estimates of the cross-isobath velocities can be made with Eq. 10 and quantities observable in the field. The velocity is greatest when the downward swimming or sinking speed of the particles is about a third of the turbulent velocity  $u^*$  or one-seventieth of the tidal current speed. Sinking speeds of  $1 \text{ cm s}^{-1}$  can lead to horizontal transports of up to a few kilometers per day given appropriate asymmetries in the strength of the vertical mixing. For a larva that can remain viable for several weeks, this implies potential motions of tens of kilometers toward the shallows. These directed transports arise with no navigation or effort on the part of the plankton—they simply sink. Directed cross-isobath transports such as these could be an important mechanism aiding the recruitment of meroplanktonic larvae to nearshore adult habitats.

## References

- BACKUS, R. H., AND D. W. BOURNE. 1987. Georges Bank. MIT Press.
- CHEN, C., AND R. C. BEARDSLEY. 1998. Tidal mixing and cross-frontal particle exchange over a finite amplitude asymmetric bank: A model study with application to Georges Bank. *J. Mar. Res.* **56**: 1163–1201.
- CHIA, F-S., J. BUCKLAND-NICKS, AND C. M. YOUNG. 1984. Locomotion of marine invertebrate larvae: A review. *Can. J. Zool.* **62**: 1205–1222.
- CULLINEY, J. L. 1974. Larval development of the giant scallop *Placopecten magellanicus* (Gmelin). *Biological Bulletin of the Marine Biological Laboratory, Woods Hole* **147**: 321–332.
- DE WOLF, P. 1973. Ecological observations on the mechanisms of dispersal of barnacle larvae during planktonic life and settling. *Neth. J. Sea Res.* **6**: 1–129.
- EMERSON, C. W. 1991. A method for the measurement of bedload sediment transport and passive faunal transport on intertidal sandflats. *Estuaries* **14**: 361–371.
- FREDSOE, J., AND R. DEIGAARD. 1992. *Mechanics of coastal sediment transport*. World Scientific.
- GALLAGER, S. M., J. L. MANUEL, D. A. MANNING, AND R. O'DOR. 1996. Ontogenetic changes in the vertical distribution of giant scallop larvae, *Placopecten magellanicus*, in 9-m deep mesocosms as a function of light, food, and temperature stratification. *Mar. Biol.* **124**: 679–692.
- GAWARKIEWICZ, G. 1993. Steady wind forcing of a density front over a circular bank. *J. Mar. Res.* **51**: 109–134.
- GEYER, W. R. 1995. Tide-induced mixing in the Amazon frontal zone. *J. Geophys. Res.* **100**: 2341–2353.
- HANSEN, AND RATTRAY. 1965. Gravitational circulation in straits and estuaries. *J. Mar. Res.* **23**: 104–122.
- HORNE, E. P. W., J. W. LODER, C. E. NAIMIE, AND N. OAKEY. 1996. Turbulence dissipation rates and nitrate supply in the upper water column on Georges Bank. *Deep-Sea Res. II* **43**: 1683–1712.
- JAY, D. A. AND J. D. MUSIAK. 1994. Particle trapping in estuarine tidal flows. *J. Geophys. Res.* **99**: 20445–20461.
- KUNDU, P. 1990. *Fluid mechanics*. Academic.
- LEVIN, L. A., AND T. BRIDGES. 1995. Pattern and diversity in reproduction and development, p. 1–48. *In* L. McEdward [ed.], *Ecology of marine invertebrate larvae*. CRC.
- LEWIS, C. V. W., C. S. DAVIS, AND G. GAWARKIEWICZ. 1994. Wind forced biological-physical interactions on an isolated offshore bank. *Deep-Sea Res.* **41**: 51–73.
- MANUEL, J. L., S. M. GALLAGER, C. M. PEARCE, D. A. MANNING, AND R. K. O'DOR. 1996. Veligers from different populations of sea scallop *Placopecten magellanicus* have different vertical migration patterns. *Mar. Ecol. Prog. Ser.* **142**: 147–163.
- MCCONAUGH, J. R. 1992. Decapod larvae: Dispersal, mortality, and ecology. A working hypothesis. *Am. Zool.* **32**: 512–523.
- NUNES VAS, R. A., AND J. H. SIMPSON. 1994. Turbulence closure modeling of estuarine stratification. *J. Geophys. Res.* **99**: 16143–16160.
- PEARCE, C. M., S. M. GALLAGER, J. L. MANUEL, D. A. MANNING, R. K. O'DOR, AND E. BOURGET. 1998. Effect of thermoclines and turbulence on depth of larval settlement and sprat recruitment of the giant scallop *Placopecten magellanicus* in 9.5 m deep laboratory mesocosms. *Mar. Ecol. Prog. Ser.* **165**: 195–215.
- SIGNELL, R. P., R. C. BEARDSLEY, H. C. GRABER, AND A. CAPOTONDI. 1990. Effect of wave-current interaction on wind-driven circulation in narrow, shallow embayments. *J. Geophys. Res.* **95**: 9671–9678.
- STULL, R. B. 1988. *An Introduction to Boundary Layer Meteorology*. Kluwer.
- TANG, K. W., H. G. DAM, AND L. R. FEINBERG. 1998. The relative importance of egg production rate, hatching success, hatching duration and egg sinking in population recruitment of two species of marine copepod. *J. Plankton Res.* **20**: 1971–1988.
- TREMBLEY, J. T. 1991. Sea scallop larvae *Placopecten magellanicus* in the Georges Bank region: Distribution, abundance and condition. Ph.D. thesis, Dalhousie University.
- TROWBRIDGE, J. H., AND S. J. LENTZ. 1998. Dynamics of the bottom boundary layer on the northern California shelf. *J. Phys. Oceanogr.* **28**: 2075–2093.
- TWICHELL, D. C., B. BUTMAN, AND R. S. LEWIS. 1987. Shallow structure, surficial geology, and the processes currently shaping

- the bank, p. 31–37. *In* R. H. Backus and D. W. Bourne [eds.], Georges Bank. MIT Press.
- VILLARET, C., AND J. H. TROWBRIDGE. 1991. Effects of stratification by suspended sediment on turbulent shear flows. *J. Geophys. Res.* **96**: 10659–10680.
- VISSER, A. W. 1997. Using random walk models to simulate the vertical distribution of particles in a turbulent water column. *Mar. Ecol. Prog. Ser.* **158**: 257–281.
- WERNER, S. R. 1999. Surface and bottom boundary layer dynamics on a shallow submarine bank: Southern flank of Georges Bank. Ph.D. thesis. MIT and Woods Hole Oceanographic Institution Joint Program.
- WILLIAMS, J. J., AND OTHERS. 1999. Field observations and predictions of bed shear stresses and vertical suspended sediment concentration profiles in wave-current conditions. *Cont. Shelf Res.* **19**: 507–536.
- WOOD, L., AND W. J. HARGIS. 1971. Transport of bivalve larvae in a tidal estuary, p. 29–44. *In* D. J. Crisp [ed.], Fourth European Marine Biology Symposium. Cambridge Univ. Press.

*Received: 1 February 2000*

*Accepted: 2 November 2000*

*Amended: 14 November 2000*